Atmos. Meas. Tech. Discuss., doi:10.5194/amt-2016-388, 2016
Manuscript under review for journal Atmos. Meas. Tech.
Published: 12 December 2016

Atmospheric Measurement Techniques Discussions
Open Access

Exploring the potential of utilizing high resolution X-band radar for urban rainfall estimation

Wen-Yu Yang[1], Guang-Heng Ni[1], You-Cun Qi[2,3], Yang Hong[1,4], Ting Sun[1*]

1) State Key Laboratory of Hydro-Science and Engineering, Department of Hydraulic Engineering, Tsinghua University, Beijing 100084, China

2) Cooperative Institute for Mesoscale Meteorological Studies, University of Oklahoma

3) NOAA/OAR/National Severe Storms Laboratory, Norman, Oklahoma

4) Department of Civil Engineering and Environmental Science, University of Oklahoma, Norman, Oklahoma

* Corresponding Author: sunting@tsinghua.edu.cn

Abstract:

X-band-radar-based quantitative precipitation estimation (QPE) system is increasingly gaining interest thanks to its strength in providing high spatial resolution rainfall information for urban hydrological applications. However, prior to such applications, a variety of errors associated with X-band radars are mandatory to be corrected. In general, X-band radar QPE systems are affected by two types of errors: 1) common errors (e.g. mis-calibration, beam blockage, attenuation, non-precipitation clutter, variations in the raindrop size distribution) and 2) "wind drift" errors resulting from non-vertical falling of raindrops. In this study, we first assess the impacts of different corrections of common error using a dataset consisting of one-year reflectivity measurements collected at an X-band radar site and a distrometer along with rainfall measurements in Beijing urban area. The common error corrections demonstrate promising improvements in the rainfall estimates, even though an underestimate of 24.6% by the radar QPE system in the total accumulated rainfall still exists as compared with gauge measurements. The most significant improvement is realized by beam integration correction. The DSD-related corrections (i.e., convective–stratiform classification and local *Z-R* relationship) also lead to remarkable improvement and highlight the necessity of deriving the localized *Z-R* relationships for specific rainfall systems. The effectiveness of wind drift correction is then evaluated for a fast-moving case, whose results indicate both the total accumulation and the temporal characteristics of the rainfall estimates can be improved. In conclusion, considerable potential of X-band radar in high-resolution rainfall estimation can be realized by necessary error

corrections.

Keywords: urban hydrology, X-band radar, quantitative precipitation estimation, error correction, wind drift effect

1. Introduction

Urban flash flooding is one of the most severe hazards in cities (Schmitt et al., 2004; Yang et al., 2015a). Large coverage of impervious surfaces in cities will exaggerate the flooding since heavy rainfall is more likely to transform into runoff instead of infiltrating into the soil. To mitigate its detrimental effects, accurate prediction of runoff at high spatiotemporal resolution is critical for emergency management and warning operations. When conducting the hydrological and/or hydraulic simulations, the spatiotemporal variability of rainfall is known to be the major source of a range of uncertainties (Schellart et al., 2012; Schröter et al., 2015; Rafieeinasab et al., 2015; Rico-Ramirez et al., 2015), which thus warrants compelling need for high-resolutions rainfall data (Schilling, 1991; Emmanuel,et al, 2012; Eldardiry et al., 2015).

Weather radars have been worldwide recognized as essential tools to provide high-resolution rainfall measurements (Smith and Krajewski, 1991; Krajewski and Smith, 2002; Li et al., 2014; Li et al., 2015). The current operational weather radar systems (e.g., NEXRAD in America, OPERA in Europe) based on C-band and/or S-band radars operating on long-range coverage. However, their spatiotemporal resolutions of 1 km/5–10 min are insufficient to support accurate estimations of precipitation variability in urban area (Krajewski et al., 2002; Smith et al., 2007). For instance, recent studies suggest that for urban areas less than 1 ha, rainfall input is required at the spatial resolution of ~100 m; while for urban areas between 1 ha and ~100 ha, the required resolution is relaxed to 500 m (Faures et al., 1995; Berne et al., 2004). Considering the high utility in monitoring rainfall in urban area, X-band radars are being deployed in a number of hydrometeorological applications (Chen and Chandrasekar, 2015).

Prior to the application of radar-based rainfall product in hydrological simulations, quantitative precipitation estimation (QPE) systems are mandatory to be established, where multiple error sources should be appreciated (e.g. Krajewski and Smith, 2002; Villarini and Krajewski, 2010). One of the error sources is associated with the reflectivity measurement, which can be attributable to mis-calibration, beam blockage, attenuation, non-precipitation clutter, and vertical profile of reflectivity (VPR). These errors may reduce the accuracy of reflectivity measured by weather radar (Germann et al., 2006; Hazenberg et al., 2011a). The variability of *Z*–*R* relationship is another important error source. The standard *Z*–*R* relationship (Chapon et al., 2008; Hazenberg et al., 2011b) takes the form of $Z = aR^b$ (Marshall and Palmer, 1948), in which the parameters a and b depend on the raindrop size distribution (DSD). Inappropriate determination of a and b will introduce errors into the estimated rainfall. The above errors are termed as **common errors** in this study as they have to be corrected for most operational radars.

Besides the common errors, the rainfall estimates for X-band radar can be affected by other weather-related dynamic processes. For instance, the falling paths of raindrops are not perfectly vertical due to wind, implying a horizontal displacement may exist between the aloft measurement position and ground falling location of a raindrop, or the **"wind drift"**. The wind drift can lead to inconsistency between the estimated and actual rainfall fields at the ground level (Fabry et al., 1994; Liu and Krajewski, 1996; Sandford., 2015; Seo and Krajewski, 2015). Usually the wind drift is ignored for the S-band and C-band radars due to their relatively coarse spatial resolution. However, this effect can be remarkable for X-band radars given its high spatial resolution of ~100 m, in particular under windy conditions that are common for convective rainfall events (Sandford, 2015; Seo and Krajewski, 2015). As such, errors due to the wind drift should be appreciated in the application of X-band radars in urban hydrometeorology.

In order to improve the quality of X-band radar based QPE systems in urban hydrometeorological applications, different procedures have been explored to reduce the aforementioned errors. Current research on X-band radar shows that using the differential phase shift can reliably resolve the attenuation which is the primary disadvantage of X-band radar (Anagnostou et al., 2004, 2006a,b; Park et al., 2005; Kalogiros et al. 2014). Specifically, Kalogiros et al. (2014) developed an algorithm to correct the attenuation of horizontal-polarization reflectivity by using an iterative optimal parameterizations of specific differential attenuation and backscattering phase shift. Besides the attenuation, Van de Beek et al. (2010) suggested that the effects of non-precipitation clutter should also be carefully addressed for applications of X-band radars in urban areas. Lo Conti et al. (2015) investigated the effect of calibration in the *Z*–*R* relationship of an X-band radar in Palermo (Italy), suggesting the high variability of the *Z*–*R* relationships determined for specific events limited its wide applicability.

Atmos. Meas. Tech. Discuss., doi:10.5194/amt-2016-388, 2016
Manuscript under review for journal Atmos. Meas. Tech.
Published: 12 December 2016

Matrosov et al. (2016) found no bright band rainfall has distinct *Z-R* relationship from those of other rain types and should be distinguished from stratiform rainfall. For operational applications, Anagnostou et al. (2010) showed that adjusting the *Z–R* relationship for mean-field bias with the K_{DP}-*R* estimates as reference is a promising technique for acquiring unbiased high resolution radar-rainfall estimates. Maki et al. (2010) developed one X-band radar QPE system for three major metropolitan areas in Japan, which may still underestimate the rainfall by ~20% compared with the gauge measurement even though the effects due to non-precipitation clutter, beam blockage and attenuation have been accounted for. Chen and Chandrasekar (2015) developed a high-resolution (250 m/1 min) QPE system in Dallas–Fort Worth urban area consisting of polarimetric Weather Surveillance Radar 88 Doppler (WSR-88D) and X-band radars, which demonstrated low overall biases and normalized standard errors in rainfall accumulation products of different temporal scales (5-60 min). Although these studies demonstrate the effectiveness of different measures in improving the X-band-radar-based QPE systems, the relative importance of different error sources contributing to the overall errors remains to be unknown. Furthermore, given the errors of a specific radar QPE system strongly depend on the spatiotemporal characteristics of the local rainfall system, an analysis of long-term rainfall characteristics is expected to enable a better understanding of the potential of X-band-radar-based QPEs in urban hydrometeorological applications.

In this study, we use a dataset consisting of one-year measurements by an X-band radar in Beijing to explore its potential in high resolution rainfall estimation. The study period extends from July 2014 to September 2015 with 43 rainfall events. Specifically, we aim to answer the following two questions: 1) What is the relative importance of different error sources for the overall accuracy of a QPE in urban area; 2) What are the impacts of wind drift on the ground-level rainfall estimation?

The paper is organized as follows. Section 2 describes the study area and the dataset. Section 3 details the correction procedures for common error sources and wind drift in X-band-radar-based QPEs. The relative importance of correcting each common error for rainfall estimation is discussed in Section 4, followed by a case study to show the implication of wind drift correction. Finally, the concluding remarks are provided in Section 5.

2. Study Area and Data Description

Beijing, the capital city of China with more than 21 million residents, features complex topography, with mountains to its north and west and a highly urbanized area in its eastern part. Beijing is prone to summertime heavy rainfall events that occasionally lead to severe flash floods (Yang et al., 2014b).

The dataset used in this study consists of one-year measurements by a single-polarized X-band radar (Fig. 1a, hereafter referred as Beijing Radar) in the northwest of Beijing. Technical specifications of the Beijing X-band radar are given in Table 1. A full

Atmos. Meas. Tech. Discuss., doi:10.5194/amt-2016-388, 2016
Manuscript under review for journal Atmos. Meas. Tech.
Published: 12 December 2016

Atmospheric Measurement Techniques Discussions

volumetric scanning by the Beijing Radar is performed every 7 min at 14 elevations (0.5°, 0.9°, 1.3°, 1.8°, 2.4°, 3.1°, 4.0°, 5.1°, 6.4°, 8, 10.0°, 12.0°, 15.6°, and 19.5°). Each scan has 400 gates along the beam with a gate resolution of 90 m and a maximum range of 36 km.

An OTT Parsivel disdrometer (Fig.. 1b) deployed near the Beijing Radar (within 5 km, cf. Fig. 2) and a gauge network consisting of 8 standard tipping-bucket gauges (Fig. 2) are used to validate the QPE system for Beijing Radar. The disdrometer can archive 32 equivalent diameter classes (ranging from 0 to 26 mm with varying diameter increments between 0.125 and 3 mm) and 32 different velocity classes at 1-min resolution. Other specifications of the disdrometer are provided in Table 2.

In order to avoid the temporal bias among radar, disdrometer and rain gauge measurements, all the measurements are conformed at 1-h resolution for subsequent analysis. We note that the bias correction by assimilating gauge data were not performed in this study due to its shadow effect over the corrections in radar QPE system (Hazenberg et al., 2011a).

3. Rainfall estimation algorithm

3.1 Procedures for common error corrections

The common errors introduced in reflectivity measurement are mostly due to radar miscalibration, non-precipitating echo contamination, signal attenuation, beam blockage and VPR, whereas the errors in *Z-R* conversion rely on the variability in *Z-R* relationships for different rainfall types. We note that the errors due to VPR are not considered for two reasons: 1) the lack of required a priori knowledge of vertical profile of rainfall in Beijing and 2) the minimal influence of VPR in this study since the maximum effective measurement height of 2.5 km of Beijing Radar is lower than the melting layer height of ~4 km for the warm-season rainfall (Cao and Qi, 2014).

3.1.1 Radar calibration

Radar calibration is conducted to fix the inappropriate parameter settings. Although the Beijing Radar has been calibrated before installation, post-installation calibration should be conducted to cancel the possible aging and thermal effects (Collier, 1989). Among all the available calibration approaches (Manz et al., 2000), calibration with disdrometer data would be the most straightforward one (Lee and Zawadzki, 2006). With the help of a nearby disdrometer (cf. Fig. 2 for its location), Beijing Radar is calibrated by comparing the radar measurements with disdrometer measurements. The disdrometer-based estimate of Z can be expressed as (Delrieu et al., 1999):

$$Z = \frac{10^6 \lambda^4}{\pi^5 |K|^2} \int_0^\infty \sigma_B(D) N(D) dD, \quad (1)$$

where λ is the operational wavelength of the radar (3.21 cm in this study), $|K|^2$ a coefficient dependent on the dielectric constant of water. Assuming a raindrop is a sphere of diameter D (cm), DSD spectra $N(D)$ (cm^{-4}) is defined as the raindrop concentration in a given air volume as a function of D and $\sigma_B(D)$ is the backscattering cross-section area (cm^2) as a function of D. Note that the Mie calculation is adopted in this study since the Rayleigh approximation does not satisfy the condition $D \leq \lambda/16$ when $\lambda = 3.21$ cm.

The comparison of the reflectivity measurement between radar and disdrometer demonstrates overall consistency with observed underestimates by radar for reflectivity exceeding 35 dBZ (an example for the comparison of the 1th September 2014 event is shown in Fig. 3). Except for the calibration error, this underestimation may be the joint effect of attenuation and inconsistency between the ground-level point measurements and the aloft volume measurements. Therefore, although there is a calibration drift for the Beijing Radar, it was decided not to apply any correction to the reflectivity measurements for the 43 selected events.

3.1.2 Non-precipitating echo removal

Radar echoes may be contaminated by non-precipitating echoes that need to be identified and removed before rainfall estimation. Ground clutters and anomalous propagations are the two main sources of non-precipitating echoes (Steiner and Smith, 2002). Ground clutters are caused by scattering in the antenna sidelobes hitting the ground close to the radar site as well as by fixed objects (Villarini and Krajewski, 2010). Anomalous propagations are contamination of radar reflectivity data from echoes normally not seen by the radar. In particular, anomalous propagations remain a serious problem for situations when they are embedded in precipitation echoes (Steiner and

Atmos. Meas. Tech. Discuss., doi:10.5194/amt-2016-388, 2016
Manuscript under review for journal Atmos. Meas. Tech.
Published: 12 December 2016

Smith, 2002).

For Beijing Radar, the ground clutter effect is corrected by removing the echoes with radial Doppler velocity close to zero. As the more advanced polarimetric techniques cannot be applied to the measurements by the Beijing Radar, the well-recognized Steiner and Smith (2002) algorithm is used for detecting anomalous propagations (e.g., Hazenberg et al., 2011a, Hazenberg et al., 2014). This algorithm utilizes the three-dimensional reflectivity structure and builds upon three key parameters: the vertical extent of radar echoes, their spatial variability and vertical gradient of intensity, which are available in the Beijing Radar measurements.

3.1.3 Attenuation correction

Radar signals can be attenuated during propagation (Atlas and Banks, 1951), in particular for X-band radars running at short wavelengths. For single-polarized radars, correction algorithms can be categorized into forward and backward algorithms (Delrieu et al., 1999). Among the forward algorithms, the HB algorithm (Hitschfeld and Bordan, 1954) is widely applied and thus adopted in this study for attenuation correction, whose key steps are recapitulated here.

For a well calibrated radar without blind-range attenuation (e.g. radome attenuation), its measured reflectivity Z_m can be expressed as:

$$Z_m(r) = Z(r)\,A(r), \quad (2)$$

Atmos. Meas. Tech. Discuss., doi:10.5194/amt-2016-388, 2016
Manuscript under review for journal Atmos. Meas. Tech.
Published: 12 December 2016

where *Z*(*r*) is the true reflectivity at the same range and $A(r) = \exp\left(-\frac{2\,ln(10)}{10}\int_0^r k(s)ds\right)$ is the path-integrated attenuation (PIA) factor with the specific attenuation *k*(*s*) at a distance *s* being the only unknown to resolve.

Meanwhile the relationship between the true reflectivity *Z* and the specific attenuation *k* can be given by:

$$Z = ck^d, \quad (3)$$

where *c* and *d* are the DSD related parameters. Therefore, by canceling *k*, the relationship between $Z_m(r)$ and $Z(r)$ can be obtained as follows:

$$Z(r) = \frac{Z_m(r)}{\left(1 - \frac{2\,ln(10)}{10}\int_0^r \left(\frac{Z_m(s)}{c}\right)^{\frac{1}{d}} ds\right)^d}, \quad (4)$$

where the parameters *c* and *d* can be determined by *Z*-*k* regression (Eq.3) with distrometer measurements. To avoid the numeric instability known in the HB algorithm, a maximum PIA of 10 dB is specified in this study.

Also, knowing the DSD, *k* can be calculated by:

$$k = c_k \int_0^\infty Q_t(D)N(D)dD, \quad (5)$$

where *D* (cm) denotes the raindrop diameter, Q_t (cm^2) the Mie total attenuation cross sections (refer to Delrieu et al. (1999) for the calculation method of Q_t), *N* (cm^{-4}) the raindrop concentration in a given air volume and $c_k = 0.4343 \times 10^6$ a constant.

By conducting *Z*-*k* regression (Eq. 3) with distrometer measurements from July 2014 to September 2015 without differentiating rainfall types (Fig. 4), the required parameters for Z_m-Z relationship (Eq.4) are determined as $c = 1.12 \times 10^5$ and $d = 1.1$.

3.1.4 Beam Integration

Due to the presence of obstructions on the beam path in terrain-complex contexts (e.g. urban, mountainous areas), beam blockage frequently occurs and thus compromise the accuracy of radar QPE. In particular, considering the radar are usually operated at the low elevation angles where more ground clutters exist, removal of beam blockage effect is of great importance for radar QPE systems. As such, beam integration, a technique to avoid the beam blockage by integrating measurements at different elevations for different azimuths, is conducted in this study.

In this study, the starting integral elevation, or the lowest optimal elevation, for a specific azimuth range is determined as the lowest elevation that at which the beam blockage of all ranges in this azimuth range must be less than 50% (cf. Fig. 2 for the starting integral elevations in this study). For instance, measurements at the elevation of 4.0 ° for the azimuth between 177 ° and 181 ° are used in this study since two tall buildings stand to the south of the Beijing Radar.

3.1.5 Convective–stratiform classification

Because of the distinct DSD characteristics between the convective and stratiform

Atmos. Meas. Tech. Discuss., doi:10.5194/amt-2016-388, 2016
Manuscript under review for journal Atmos. Meas. Tech.
Published: 12 December 2016

rainfall, the *Z-R* relationships for the two types of rainfall differ significantly. It is thus necessary to conduct the convective-stratiform classification before the *Z-R* conversion. Due to the unavailability of real-time atmospheric temperature profiles that is commonly used for convective-stratiform classification, a vertically integrated liquid (VIL; Greene and Clark, 1972) based method (Zhang and Qi, 2010) is adopted in this study.

With the volume scan reflectivity measurements, VIL can be obtained by:

$$\mathrm{VIL} = \sum_k \mathrm{VILpar_k}, \quad (6)$$

where $\mathrm{VILpar}_k = \mathrm{LW} \cdot \mathrm{DB}$ denotes the VIL within the k^{th} tilt with LW (kg km^{-3}) and DB (km) being the liquid water content associated with a particular value of reflectivity and the depth of a radar beam, respectively, given by

$$\mathrm{LW} = 3.44 \times 10^3 Z^{\frac{4}{7}}, \quad (7)$$

$$\mathrm{DB} = \begin{cases} \mathrm{BH}\left[\theta_{k_{top}} + 0.5\mathrm{BW}\right] - \mathrm{BH}\left[0.5\left(\theta_{k_{top}} + \theta_{k_{top}-1}\right)\right] & k = k_{top} \\ \mathrm{BH}[0.5(\theta_{k+1} + \theta_k)] - \mathrm{BH}\left[0.5\left((\theta_k + \theta_{k-1})\right)\right] & 1 < k < k_{top}, \\ \mathrm{BH}\left[0.5\left((\theta_1 + \theta_2)\right)\right] & k = 1 \end{cases} \quad (8)$$

where DB (km) is the depth of a radar beam, *Z* the radar reflectivity within a radar sample volume, BW the angular width of the radar beam between the half-power points, BH the beam center height for a given elevation angle and range under the standard atmospheric refraction conditions and θ_k the elevation angle at the k^{th} tilt.

Once the knowledge of VIL is obtained, the reflectivity pixels can be categorized into stratiform with $\mathrm{VIL} < 6.5\ \mathrm{kg\ m^{-2}}$ and convective with $\mathrm{VIL} \geq 6.5\ \mathrm{kg\ m^{-2}}$.

3.1.6 Derivation of local *Z-R* relationships

The standard *Z-R* relationships are $Z = 200\ R^{1.6}$ and $Z = 300\ R^{1.4}$ for stratiform and convective situations, respectively. However, due to the large variability of *Z-R* relationship among different locations, localized *Z-R* relationships are mandatory for building radar QPE systems. As such, we use the DSD measurements collected at the distrometer sites near the Beijing Radar to establish the local *Z-R* relationships.

As can be seen in Fig. 5, by conducting *Z-R* regression without differentiating rainfall types, Z=428.4 $R^{1.2}$ is obtained from non-linear regression. Furthermore, considering the rainfall types (stratiform for $Z \leq 39$ dBZ and convective for $Z > 39$ dBZ; cf. Steiner et al., 1995), *Z-R* relationships Z=426.5 $R^{1.3}$ and Z=499.3 $R^{1.2}$ are obtained for stratiform and convective event, respectively. It is noteworthy that the *Z-R* relationships derived by this study distinguish from the standard forms, implying the necessity of locally-derived forms in radar QPE systems. It is also noteworthy the convective events comprise a large portion of the rainfall events, which is consistent with the previous findings that convective events are common in urban areas. (Yang et al., 2014a, Yang et al., 2015b, Yu et al., 2015).

3.2 Procedure for wind drift correction

Wind drift means the horizontal displacement between the aloft measurement position and ground falling location of a raindrop. Wind drift correction enables better rainfall

Atmos. Meas. Tech. Discuss., doi:10.5194/amt-2016-388, 2016
Manuscript under review for journal Atmos. Meas. Tech.
Published: 12 December 2016

estimation at the ground level. The horizontal displacement Δx of a raindrop can be estimated by integrating horizontal wind velocity $u(h)$ over falling duration (Caroline, 2015) as follows:

$$\Delta x = \int_0^t u(h)dt = \int_0^{h_b} \frac{u(h)}{w(h)} dh, \tag{9}$$

where $w(h)$ is the falling speed at height h and h_b is the height of the radar beam at the measurement location. And $u(h)$ is given by:

$$u(h) = S \cdot h, \tag{10}$$

where S is a constant wind shear (Caroline, 2015).

By assuming a zero wind speed at the ground level, the wind shear S can be calculated by:

$$S = \frac{u(h_b)}{h_b}. \tag{11}$$

Given the constant falling speed of 5 m s^{-1} for raindrops blow the melting layer (Caroline 2015), the Eq. (12) thus can be simplified as:

$$\Delta \mathrm{x} = \frac{1}{5}\frac{Sh_b^2}{2} = \frac{u(h_b)h_b}{10}. \tag{12}$$

Furthermore, $u(h_b)$ can be determined by a pixel-based tracking algorithm for short-term quantitative rainfall forecasting (Zahraei et al., 2012). The tracking algorithm can estimate the advection velocity of a rainy pixel (equal to the background wind velocity) by tracking its successive positions between radar images based on the maximum correlation of meshes in consecutive images.

4. Results and discussion

4.1 Importance of different common corrections

Atmos. Meas. Tech. Discuss., doi:10.5194/amt-2016-388, 2016
Manuscript under review for journal Atmos. Meas. Tech.
Published: 12 December 2016

Atmospheric Measurement Techniques Discussions

To assess the relative importance of different common error corrections, a rotation-based strategy is conducted, which consists of two procedures as follows:

1) **Complete-correction (CC) procedure**: all the corrections described in Section 3.1 are applied to the reflectivity measurements to obtain the rainfall field as the best estimate;
2) **Partial-correction (PC) procedure**: all but one of the corrections as in the CC procedure are used to estimate the rainfall, whereby the corresponding estimate can be compared with the best estimate of CC procedure to assess the effectiveness of a specific error correction (i.e., the excluded correction). By rotating the specific correction in the PC procedure, rainfall estimates without different corrections can thus be obtained.

Furthermore, to quantify the correction effectiveness so that get the relative importance of different error sources contributing to the overall errors, the radar-gauge ratio of daily accumulated rainfall *rd*, average radar-gauge ratio of total rainfall *ra*, the root-mean-square error RMSE, and the coefficient of determination r^2 are introduced as follows:

$$rd_{i,k} = \sum_n R_{n_{i,k}} / \sum_n G_{n_{i,k}}, \tag{13}$$

$$ra = \frac{1}{8}\sum_{k=1}^{8} \sum_n R_{n,k} / \sum_n G_{n,k}, \tag{14}$$

$$\mathrm{RMSE} = \sqrt{\frac{1}{N}\sum_{n=1}^{N}(R_n - G_n)^2}, \tag{15}$$

$$\mathrm{r}^2 = \frac{\left(\sum (R_n - \overline{R_n})(G_n - \overline{G_n})\right)^2}{\left(\sum_{n=1}^{N}(R_n - \overline{R_n})^2\right)\left(\sum_{n=1}^{N}(G_n - \overline{G_n})^2\right)} \tag{16}$$

where the subscript *i* and *k* denote the date number and gauge number, respectively; while the radar-based estimates *R* and gauge measurements *G* with n and N denoting the n-th hour and total number of hours, respectively. The first two metrics are chosen to describe the systematic bias, while the last two assess the average error magnitude and agreement at hourly scale.

To reduce the bias in the radar-gauge comparison, 33 events, during which at least three gauges have valid measurements, are chosen and investigated for the correction effectiveness. For the 33 events, the ratio *rd* based on the CC procedure varies mostly between 0 and 3 with the medians ranging between 0.5 and 1.5 (Fig. 6), suggesting a promising performance of common corrections, though considerable variability can be observed for several events (e.g., events of July 29, 2015). Extending beyond the 33 chosen events to all the events in the study period, it is also noted that with the CC procedure performed, the Beijing Radar underestimates the rainfall compared with the gauges (cf. a linear radar-gauge regression slope of 0.69 and coefficient of determination R^2 of 0.76 in Fig. 7) with an averaged underestimate of 24.6% in the total rainfall. This result is comparable with that of the X-band radar at the Delft University (cf. a linear radar-gauge regression slope of 0.65 reported in Van de Beek et al. (2010)).

The influence of the PC procedure on the rainfall estimates is then examined by comparing the above metrics between the radar-based estimates and gauge measurements during the study period (Table 3 and Fig. 8). Correction for anomalous propagations contributes a minimal improvement in the rainfall estimates (Fig. 8a) because this correction may reduce the estimated reflectivity and thus the rainfall.

Atmos. Meas. Tech. Discuss., doi:10.5194/amt-2016-388, 2016
Manuscript under review for journal Atmos. Meas. Tech.
Published: 12 December 2016

However, such minimal influence does NOT suggest the non-necessity of anomalous propagation correction since its improvement is largely screened by errors from other sources. The attenuation correction demonstrates improvement in the rainfall estimates in terms of both *ra* and RMSE (Fig. 8b). As expected, the largest improvement is resulted from the beam integration as indicated by the reduced RMSE (cf. RMSE from 3.18 for -BI to 1.95 for CC in Table 3) and by the increased coefficient of determination r^2 for the radar-gauge linear regression (cf. from 0.54 to 0.76 in Fig. 8c). The increased deviation for no beam integration suggests that larger *ra* (cf. 0.87 for -BI in Table 3) is actually the results of offset of positive and negative deviations.

Furthermore, significant improvements are observed in the estimated rainfall when the variability in the DSD is taken into account: both the convective–stratiform classification and the local *Z-R* relationship derivation contribute to increases in *ra* and decreases in RMSE (Table 3). Such improvements are also demonstrated by the increases in the slope of radar-gauge linear regression (Fig. 8d and e).

In general, the DSD-related corrections (i.e., convective–stratiform classification and the local *Z-R* relationship) demonstrates greater improvement in the estimation of rainfall as compared with some of the reflectivity-related corrections (i.e., anomalous propagations removal, attenuation correction), implying the importance of appropriate DSD-related corrections.

4.2 Case study: a fast-moving event of 20150904

Although considerable improvements can be observed in the rainfall estimates after the common error corrections, it should be noted the potential for improving the rainfall estimates may be realized by correcting the wind drift errors in radar QPE systems, in particular for X-band radars of high spatial resolutions. To examine the effect on the radar based rainfall estimates of wind drift correction, a long-duration event (~16 h) on 4th September 2015 featuring fast-moving storms with complex structures is analyzed here.

The event originated from low pressure system passing over Beijing from southwest towards northeast, where a high pressure zone resided over the urban area of Beijing. Taking an episode of ~30 min for instance, several convective cells rapidly grew in the southwest of Beijing (Fig. 9a and b), then quickly moved to northeast (Fig. 9c), and developed to a widespread precipitating system afterwards (Fig. 9d).

The influence of the wind drift correction on the hourly rainfall estimates is then examined by a radar-gauge linear regression (Fig. 10). After the wind drift correction, the slope and coefficient of determination R^2 of the radar-gauge regression increase from 0.46 to 0.58 and from 0.69 to 0.79, respectively, suggesting an evident improvement in the estimates of total rainfall. In addition, the temporal characteristics of rainfall estimates are refined as well. For instance of a gauge close to the radar, the correlation coefficient of the rainfall series between the radar and gauge is increased from 0.79 to 0.86 and the RMSE of rainfall measurements is reduced from 27.4 to 18.8 after the wind drift correction (Fig. 11). It is also noteworthy that the wind drift correction leads to an improved temporal consistency in the rainfall time series between the gauge and radar with the more accurate rainfall estimate at the peaking time (i.e., 17:00 shown in Fig. 11).

5. Concluding remarks

In this study, we analyzed 43 rainfall events between July 2014 and September 2015 based on the measurements gathered by an X-band single-polarized radar, a distrormeter and 8 rain gauges in Beijing urban area. These measurements allow us to explore the potential for high-resolution rainfall measurement with X-band radar over complex urban region. The impacts and importance of common corrections (i.e., radar calibration, non-precipitating echo removal, attenuation correction, beam integration, convective–stratiform classification and local *Z-R* relationships) on the quality of the radar QPE is first studied, followed by an assessment of the effectiveness of wind drift correction. The major findings are summarized as follows:

1) Although the radar QPE system underestimates the total rainfall accumulations by 24.6% as compared with gauges, the common corrections demonstrate promising improvements in the rainfall estimates.
2) The greatest improvements in the radar based rainfall estimates can be attributed to the beam integration, which significantly outperforms the operation at the single lowest elevation without beam blockage (i.e., 4.0 °in this study). It is thus highly

suggested to conduct volumetric reflectivity measurements with the X-band radar in particular for complex-terrain regions. Minor improvements on the radar rainfall estimation are observed after the anomalous propagations removal as compared to other common error corrections.

3) The DSD-related corrections (i.e., convective–stratiform classification and local *Z-R* relationship) lead to significant improvements in the rainfall estimates. And the local *Z-R* relationship plays a more crucial role in improving the rainfall estimates compared with the other corrections, which highlights the necessity of deriving the localized *Z-R* relationships for different types of rainfall.
4) The wind drift correction improve both the total accumulation and the temporal characteristics of the estimated rainfall, which suggest the necessity of wind drift correction for X-band radars of high spatial resolutions.

The possible future improvement relies on the inclusion of vertical profile of reflectivity (VPR) measurements of this region to correct the underestimation in reflectivity (Qi et al., 2013). In addition, polarimetric radars, featuring the ability to capture two-dimensional structure of rainfall, can provide new insight into rainfall microphysics and make further improvements in monitoring urban rainfall.

Acknowledgement

This work is supported by the National Science Foundation of China under grant no.

Atmos. Meas. Tech. Discuss., doi:10.5194/amt-2016-388, 2016
Manuscript under review for journal Atmos. Meas. Tech.
Published: 12 December 2016

51190092 and 51409147, by the Ministry of Science and Technology of China under Grant No. 2013DFG72270, and by China Postdoctoral Science Foundation under grant no. 2015T80093. We are grateful to the Beijing Water Authority for the assistance in providing the rain gauge data.

Atmos. Meas. Tech. Discuss., doi:10.5194/amt-2016-388, 2016
Manuscript under review for journal Atmos. Meas. Tech.
Published: 12 December 2016

References:

Anagnostou, E.N., Anagnostou, M.N., Krajewski, W.F., Kruger, A., Miriovsky, B.J.: High-resolution rainfall estimation from X-band polarimetric radar measurements, J. Hydrometeorol., 5, 110-128, 2004.

Anagnostou, E.N., Grecu, M., Anagnostou, M.N.: X-band polarimetric radar rainfall measurements in keys area microphysics project, J. Atmos. Sci., 63, 187– 203, 2006a.

Anagnostou, M.N., Anagnostou, E.N., Vivekananda, J.: Correction for rainpath specific and differential attenuation of X-band dual-polarization observations, IEEE Trans. Geosci. Remote Sens., 44, 2470–2480, 2006b.

Anagnostou, M.N., Kalogiros, J., Emmanouil, N., Anagnostou, Tarolli, M., Papadopoulos, A., Borga,M: Performance evaluation of high-resolution rainfall estimation by X-band dual-polarization radar for flash flood applications in mountainous basins, J. Hydrol., 394, 4–16, 2010.

Atlas, D., Banks, H.C.: The interpretation of microwave reflections from rainfall, J. Meteor., 8, 271–282, 1951.

Berne, A., Delrieu, G., Creutin, J., and Obed, C.: Temporal and spatial resolution of rainfall measurements required for urban hydrology, J. Hydrol., 299, 166-179, 2004.

Berne, A., Uijlenhoet, R.: Quantitative analysis of X-band weather radar attenuation correction accuracy, Nat. Hazards Earth Syst. Sci., 6, 419–425, 2006.

Cao, Q., Qi, Y.: The variability of vertical structure of precipitation in Huaihe River Basin of China: Implications from long-term spaceborne observations with TRMM precipitation radar, Water Resour. Res., 50, 3690–3705, 2014.

Atmos. Meas. Tech. Discuss., doi:10.5194/amt-2016-388, 2016
Manuscript under review for journal Atmos. Meas. Tech.
Published: 12 December 2016

Atmospheric Measurement Techniques Discussions
Open Access
EGU

Chapon, B., Delrieu, G., Gosset, M., Boudevillain, B.: Variability of rain drop size distribution and its effect on the Z–R relationship: A case study for intense Mediterranean rainfall, Atmos. Res., 87, 52-65, 2008.

Chen, H., Chandrasekar, V.: The quantitative precipitation estimation system for Dallas–Fort Worth (DFW) urban remote sensing network, J. Hydrol., 531, 259-271, 2015.

Collier, C.G.: Applications of Weather Radar Systems: A Guide to Uses of Radar data in Meteorology and Hydrology. Ellis Horwood Limited Publisher, 1989.

Delrieu, G., Caoudal, S., Creutin, J.D.: Feasibility of using mountain return for the correction of ground-based X-Band weather radar, J. Atmos. Oceanic Technol., 14, 368–385, 1997.

Delrieu, G., Hucke, L., Creutin, J.D.: Attenuation in rain for X-and C-band weather radar systems: Sensitivity with respect to the drop size distribution, J. Appl. Meteorol., 38, 57-68, 1999.

Eldardiry, H., Habib, E., Zhang, Y.: On the use of radar-based quantitative precipitation estimates for precipitation frequency analysis, J. Hydrol., 531, 441-453, 2015.

Emmanuel, I., Andrieu, H., Leblois, E., Flahaut, B.: Temporal and spatial variability of rainfall at the urban hydrological scale, J. Hydrol., 430, 162– 172, 2012.

Fabry, F., Bellon, A., Duncan, M.R., Austin, G.L: High resolution rainfall measurements by radar for very small basins: the sampling problem reexamined, J. Hydrol., 161, 415–428, 1994.

Faures, J.M., Goodrich, D., Woolhiser, D.A., Sorooshian, S.: Impact of smallscale spatial rainfall variability on runoff modeling, J. Hydrol., 173, 309–326, 1995.

Germann, U., Galli, G., Boscacci, M., Bolliger, M.: Radar precipitation measurement in a mountainous region, Q. J. R. Meteorol. Soc., 132, 1669–1692, 2006.

Greene, D.R., Clark, R.A.: Vertically integrated liquid water: a new analysis tool, Mon. Weather Rev., 100, 548–552, 1972.

Hazenberg, P., Leijnse, H., Uijlenhoet, R.: Radar rainfall estimation of stratiform winter precipitation in the Belgian Ardennes, Water Resources Res., 47, W02507, 2011a.

Hazenberg, P., Yu, N., Boudevillain, B., Delrieu, G., Uijlenhoet, R.: Scaling of raindrop size distributions and classification of radar reflectivity–rain rate relations in intense Mediterranean precipitation, J. Hydrol., 402, 179–192, 2011b.

Hazenberg, P., Leijnse, H., Uijlenhoet, R.: The impact of reflectivity correction and accounting for raindrop size distribution variability to improve precipitation estimation by weather radar for an extreme low-land mesoscale convective system, J. Hydrol., 519, 3410-3425, 2014.

Hitschfeld, W., Bordan, J.: Errors inherent in the radar measurement of rainfall at attenuating wavelengths, J. Meteor., 11, 58–67, 1954.

Kalogiros, J., Anagnostou, M. N., Anagnostou, E. N., Montopoli, M., Picciotti, E., & Marzano, F. S.: Evaluation of a new polarimetric algorithm for rain-path attenuation correction of X-band radar observations against disdrometer, IEEE Trans. Geosci. Remote Sens., 52(2), 1369-1380, 2014.

Krajewski, W.F., Smith, J.A.: Radar hydrology: rainfall estimation, Adv. Water Resour., 25, 1387-1394, 2002.

Lee, G., Zawadzki, I.: Radar calibration by gage, disdrometer, and polarimetry: theoretical limit caused by the variability of drop size distribution and application to fast scanning operational radar data, J. Hydrol., 328, 83–97, 2006.

Li, Z., Yang, D., Hong, Y., and Zhang, J.: Characterizing spatiotemporal variations of hourly rainfall by gauge and radar in the mountainous Three Gorges Region, J. Appl. Meteor. Climatol, 53(4), 873-889, 2014.

Li, Z., Yang, D., Hong, Y., Qi Y., Cao, Q.: Evaluation of radar-based precipitation estimates for flash flood forecasting in the Three Gorges Region, Proc. Int. Assoc. Hydrol. Sci., 368, 89-95, 2015.

Liu, C., Krajewski, W.F.: A comparison of methods for calculation of radarrainfall hourly accumulations, Water Resour. Bull., 32, 305–315, 1996.

Lo Conti, F., Francipane, A., Pumo, D., Noto, L.V.: Exploring single polarization X-band weather radar potentials for local meteorological and hydrological applications, J. Hydrol., 531, 508-522, 2015.

Maki, M., Maesaka, T., Kato, A., Shimizu, S., Kim, D. S., Iwanami, K., Tsuchiya, S., Kato, T., Kikumori, Y., Kieda, K.: X-band polarimetric radar networks in urban areas, ERAD 2010–6th European conference on radar in meteorology and hydrology, Sibiu, 6–10 September 2010.

Manz, A., Smith, A., Hardaker, P.: Comparison of different methods of end to end calibration of the UK weather radar network, Phys. Chem. Earth Part B 25 (10–12), 1157–1162, 2000.

Marshall, J.S., Palmer, W.M.K.: The distribution of raindrops with size, J. Meteorol.,

Atmos. Meas. Tech. Discuss., doi:10.5194/amt-2016-388, 2016
Manuscript under review for journal Atmos. Meas. Tech.
Published: 12 December 2016

5, 165–166, 1948.

Matrosov, S. Y., Cifelli, R., Neiman, P. J., & White, A. B.: Radar Rain-Rate Estimators and Their Variability due to Rainfall Type: An Assessment Based on Hydrometeorology Testbed Data from the Southeastern United States, J. Appl. Meteor. Climatol., 55(6), 1345-1358, 2016.

Qi, Y., Zhang, J., Zhang, P.: A real-time automated convective and stratiform precipitation segregation algorithm in native radar coordinates, Q. J. R. Meteorolog. Soc., 139, 2233-2240, 2013.

Rafieeinasab, A., Norouzi, A., Kim, S., Habibi, H., Nazari, B., Seo, D.J., Lee, H., Cosgrove, B., Cui, Z.: Toward high-resolution flash flood prediction in large urban areas–Analysis of sensitivity to spatiotemporal resolution of rainfall input and hydrologic modeling, J. Hydrol., 531, 370-388, 2015.

Rico-Ramirez, M.A., Liguori, S., Schellart, A.N.A.: Quantifying radar-rainfall uncertainties in urban drainage flow modelling, J. Hydrol., 528, 17-28, 2015.

Sandford, C.:, Correcting for wind drift in high resolution radar rainfall products: a feasibility study, J. Hydrol., 531, 284-295, 2015.

Schellart, A.N.A., Shepherd, W.J., Saul, A.J.: 2012, Influence of rainfall estimation error and spatial variability on sewer flow prediction at a small urban scale, Adv. Water Resour., 45, 65-75, 2015.

Schilling, W.: Rainfall data for urban hydrology: what do we need, Atmos. Res., 27, 5–21, 1991.

Schröter, K., Llort, X., Velasco-Forero, C., Ostrowski, M., Sempere-Torres, D.:

Implications of radar rainfall estimates using uncertainty on distributed hydrological model predictions, Atmos. Res., 100, 237–245, 2011.

Schmitt, T.G., Thomas, M., Ettrich, N.: Analysis and modeling of flooding in urban drainage systems, J. Hydrol., 299, 300-311, 2004.

Seo, B.C., Krajewski, W.F.: Correcting temporal sampling error in radar-rainfall: Effect of advection parameters and rain storm characteristics on the correction accuracy, J. Hydrol., 531, 272-283, 2015.

Smith, J.A., Krajewski, W.F.: Estimation of the mean field bias of radar rainfall estimates, J. Appl. Meteor., 30, 397–412, 1991.

Smith, J.A., Baeck, M.L., Meierdiercks, K.L., Miller, A.J., Krajewski, W.F.: Radar rainfall estimation for flash flood forecasting in small urban watersheds, Adv. Water Resour., 30, 2087–2097, 2007.

Steiner, M., Houze, RA. Jr., Yuter, S.E.: Climatological characterization of three-dimensional storm structure from operational radar and rain gauge data, J. Appl. Meteorol., 34, 1978–2007, 1995.

Steiner, M., Smith, J.A.: Use of three-dimensional reflectivity structure for automated detection and removal of nonprecipitating echoes in radar data, J. Atmos. Oceanic Technol., 19, 673-686, 2002.

Van de Beek, C.Z., Leijnse, H., Stricker, J.N.M., Uijlenhoet, R., Russchenberg, H.W.J.: Performance of high-resolution X-band radar for rainfall measurement in The Netherlands, Hydrol. Earth Syst. Sci., 14, 205-221, 2010.

Villarini, G., Krajewski, W.: Review of the different sources of uncertainty in single polarization radar-based estimates of rainfall, Surv. Geophys., 31, 107– 129, 2010.

Yang, L., Smith, J.A., Baeck, M.L., Bou-Zeid, E., Jessup, S.M., Tian, F., Hu, H.: Impact of urbanization on heavy convective precipitation under strong large-scale forcing: A case study over the Milwaukee-Lake Michigan region, J. Hydrometeorol., 15, 261-278, 2014a.

Yang, L., Tian, F., Smith, J.A., Hu, H.: Urban signatures in the spatial clustering of summer heavy rainfall events over the Beijing metropolitan region, J. Geophys. Res. Atmos., 119, 1203-1217, 2014b.

Yang, W., Li, D., Sun, T., Ni, G.: Saturation-excess and infiltration-excess runoff on green roofs, Ecol. Eng., 74, 327-336, 2015a.

Yang, W., Li, Z., Sun, T., Ni, G.: Better knowledge with more gauges? Investigation of the spatiotemporal characteristics of precipitation variations over the Greater Beijing Region, Int. J. Climatol., 36, 3607–3619, 2015b.

Yu, R., Chen, H., Sun, W.: The definition and characteristics of regional rainfall events demonstrated by warm season precipitation over the Beijing plain, J. Hydrometeorol., 16, 396-406, 2015.

Zahraei, A., Hsu, K.L., Sorooshian, S., Gourley, J.J., Lakshmanan, V., Hong, Y., Bellerby, T.: Quantitative precipitation nowcasting: a Lagrangian pixel-based approach, Atmos. Res., 118, 418-434, 2012.

Zhang, J., Qi, Y.: A real-time algorithm for the correction of bright band effects in radar-derived QPE, J. Hydrometeorol., 11, 1157–1171, 2010.

Table 1 Main specifications of X-band radar used in this study.

Parameters	Value
Frequency	9.38 Ghz
Peak transmitted power	25 kw, 38 dB gian
Antenna	1.3 m
Beam width	1.8 °
Platform	44 m above ground level

Table 2 Specifications of disdrometer used in this study.

Parameters	Value
Optical sensor wavelength	780 nm
Particle size range	0.2–5 mm (liquid precipitation), 0.2–25 mm (solid precipitation)
Particle velocity range	0.2–20 m s^{-1}
Measurement time aggregation interval setting	1 min
Precipitation intensity range	0.001–1200 mm h^{-1}
Radar reflectivity range	9.9–99 ±20% dBZ

Table 3 Impacts of the correcting different common errors on hourly accumulated rainfall.

Statistic[1]	CC procedure	PC procedure[2]				
		- AP	-Att	-BI	-Seg	-*Z-R*
ra	0.75	0.77	0.72	0.87	0.57	0.61
RMSE	1.95	1.97	2.02	3.18	2.17	2.34

Notes:

1. The statistics are calculated with hourly rainfall estimates. ra is the average radar-gauge ratio for 8 gauges and $\mathrm{RMSE} = \sqrt{\frac{1}{N}\sum_{n=1}^{N}(R_n - G_n)^2}$ is the root-mean-square error between the radar-based estimates R and gauge measurements G with n and N denoting the n-th hour and total number of hours, respectively.
2. The minus sign (-) in PC procedure indicates the exclusion of a specific correction. The correction names are simplified as follows: AP for anomalous propagations correction, Att for attenuation correction, BI for beam integration, Seg for convective–stratiform rainfall

classification, *Z-R* for local *Z-R* relationship derivation.

Figure 1 The site view of (a) the Beijing Radar and (b) the disdrometer used in this study.

Atmos. Meas. Tech. Discuss., doi:10.5194/amt-2016-388, 2016
Manuscript under review for journal Atmos. Meas. Tech.
Published: 12 December 2016

Atmospheric Measurement Techniques Discussions

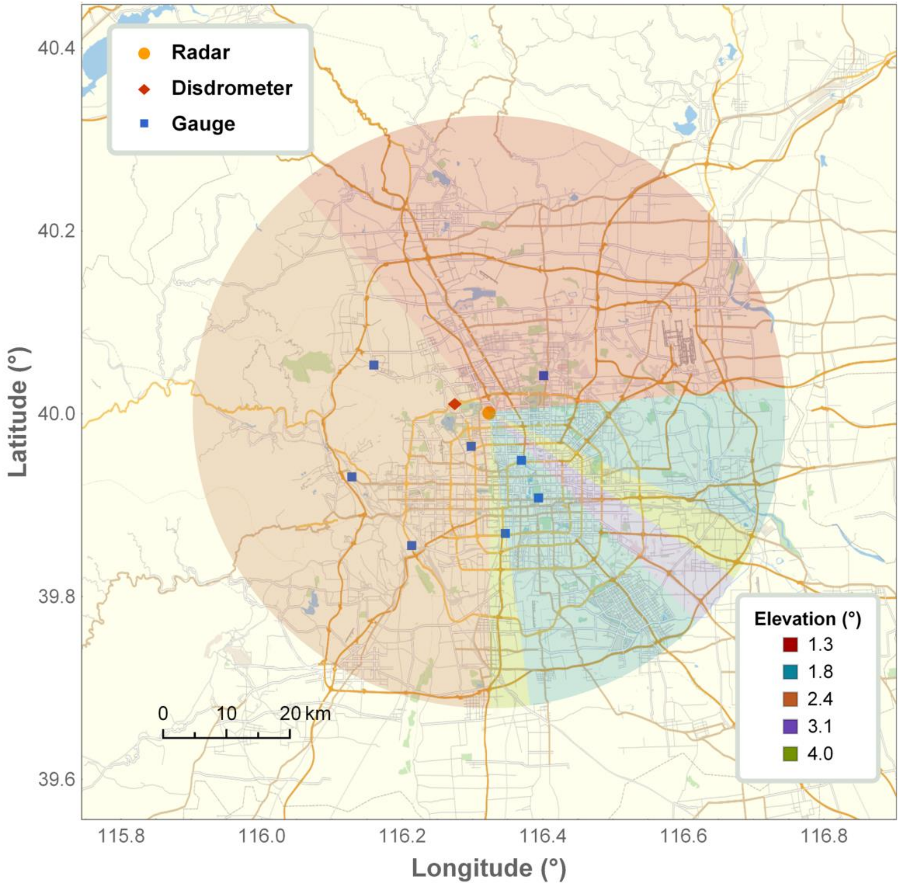

Figure 2 The instrumentation layout of urban rainfall monitoring system of in Beijing.

Atmos. Meas. Tech. Discuss., doi:10.5194/amt-2016-388, 2016
Manuscript under review for journal Atmos. Meas. Tech.
Published: 12 December 2016

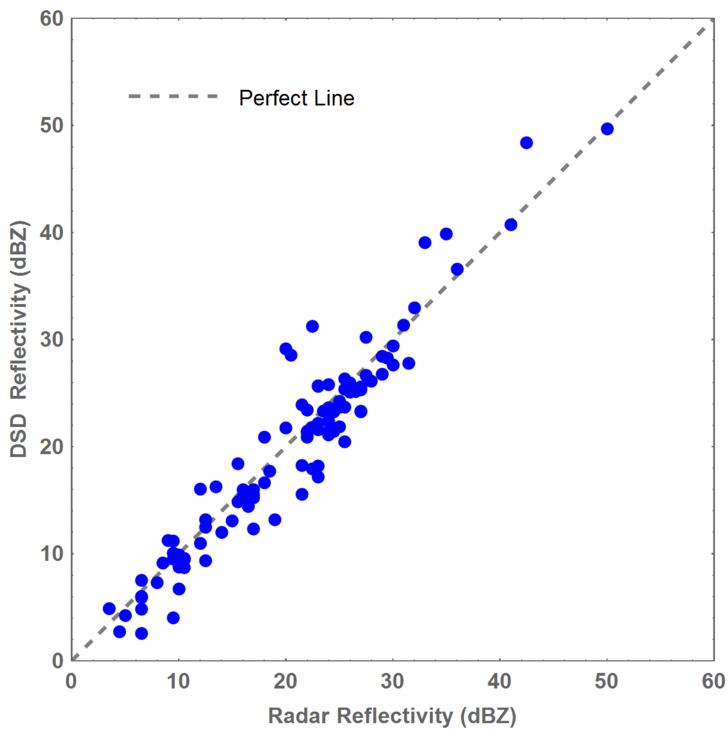

643

644 **Figure 3** The relationship between radar-measured reflectivity and distrometer-

645 estimated reflectivity.

Atmos. Meas. Tech. Discuss., doi:10.5194/amt-2016-388, 2016
Manuscript under review for journal Atmos. Meas. Tech.
Published: 12 December 2016

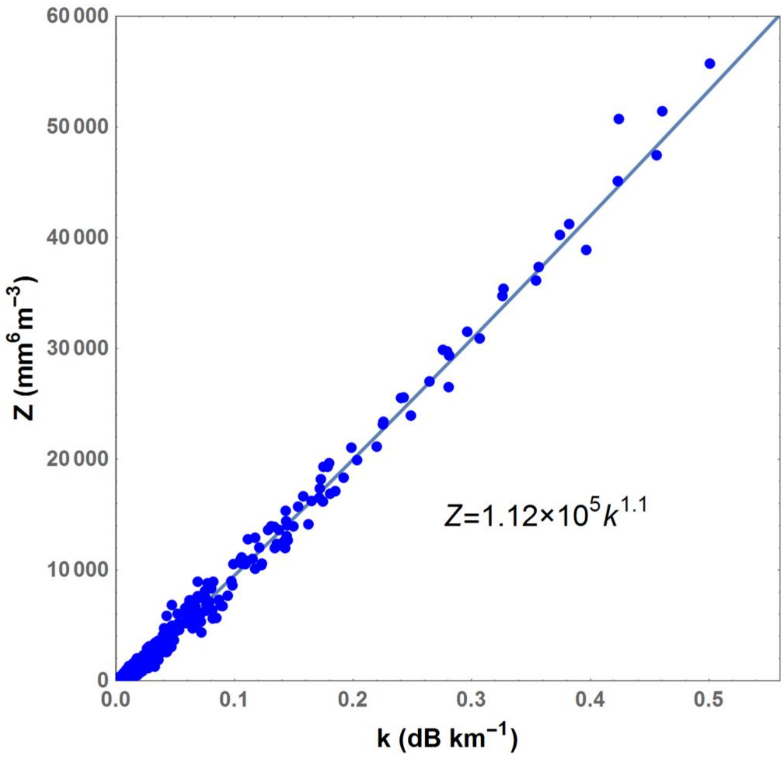

646

647 **Figure 4** *Z-k* relationship derived from DSD data using a non-linear power-law fit.

Atmos. Meas. Tech. Discuss., doi:10.5194/amt-2016-388, 2016
Manuscript under review for journal Atmos. Meas. Tech.
Published: 12 December 2016

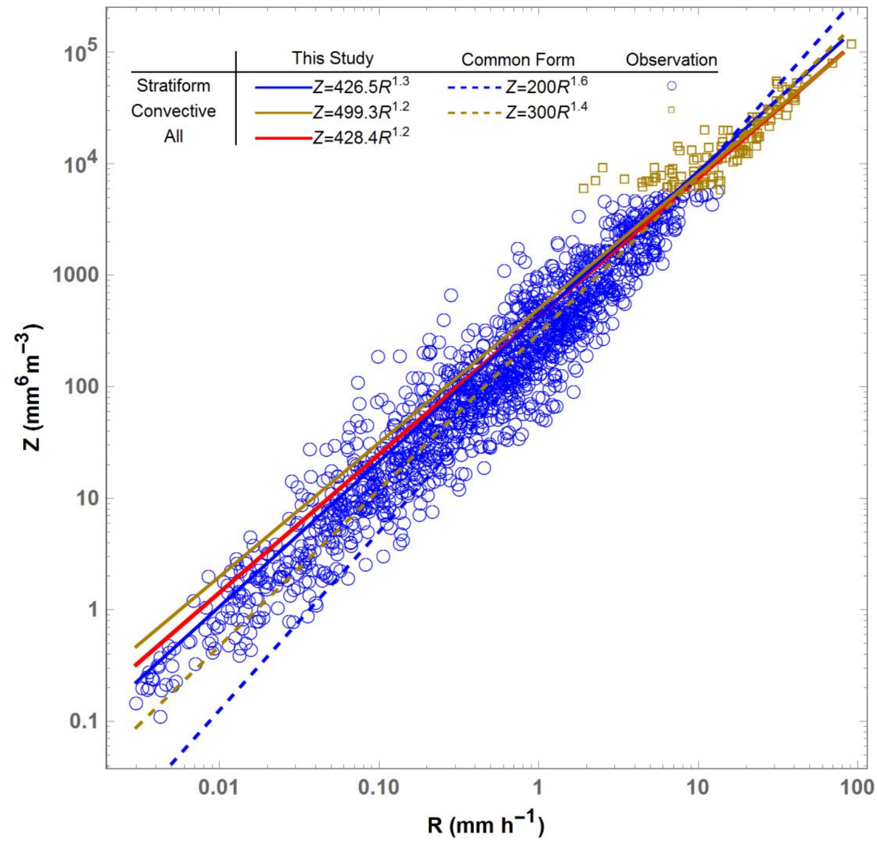

Figure 5 *Z-R* relationships for different rainfall scenarios.

Atmos. Meas. Tech. Discuss., doi:10.5194/amt-2016-388, 2016
Manuscript under review for journal Atmos. Meas. Tech.
Published: 12 December 2016

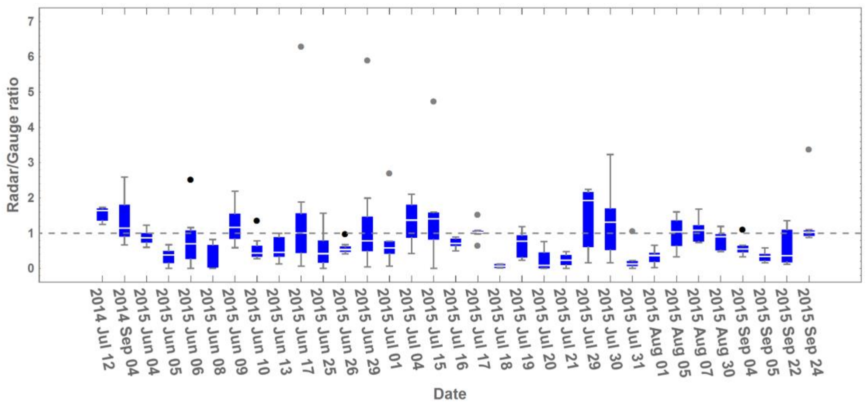

Figure 6 Radar-gauge ratios of the daily accumulated rainfall for events covering at least 3 gauges. The dots denote the outlier values. Each box ranges from the 25th percentile to the 75th percentile with the middle line denoting the median value.

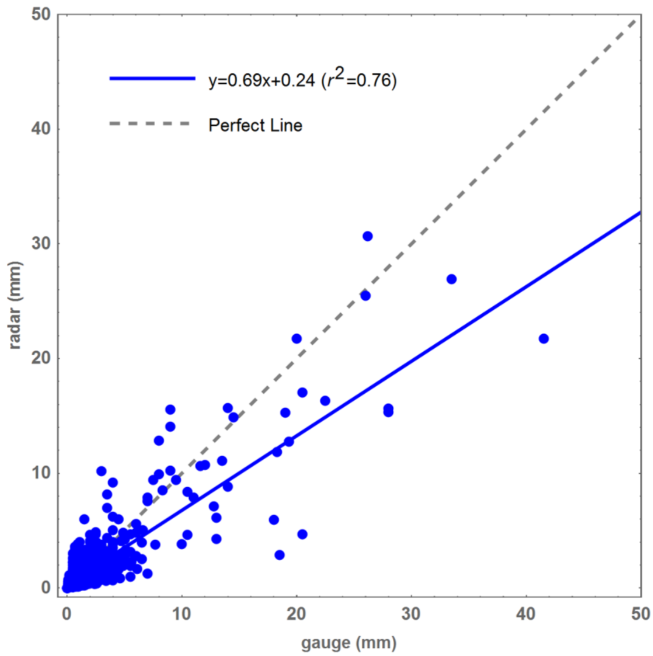

Figure 7 The relationship of hourly rainfall accumulations from 8 rain gauges and the corresponding radar pixels for all the events.

Atmos. Meas. Tech. Discuss., doi:10.5194/amt-2016-388, 2016
Manuscript under review for journal Atmos. Meas. Tech.
Published: 12 December 2016

Atmospheric Measurement Techniques
Discussions

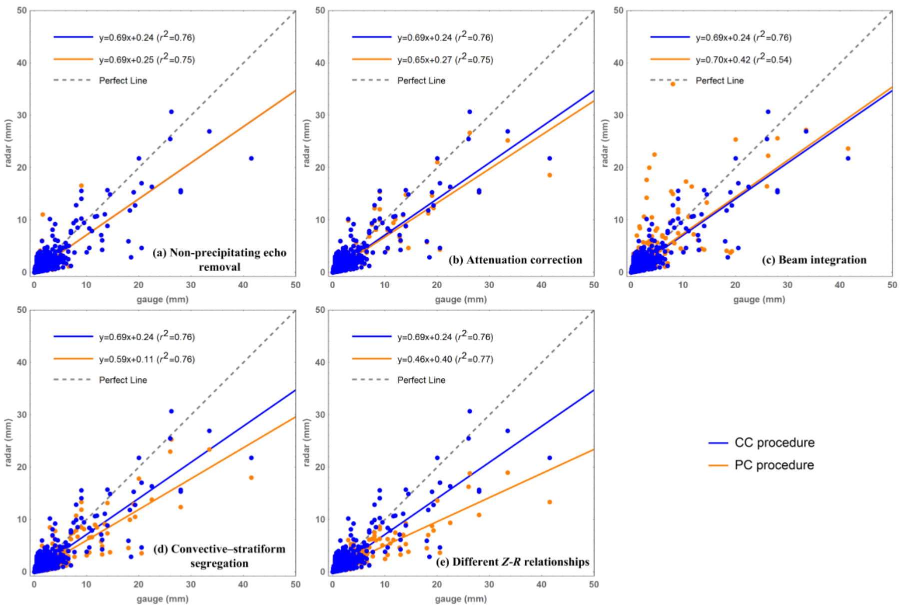

Figure 8 Performance in radar-based rainfall estimation of different corrections: (a) non-precipitation echo removal, (b) attenuation correction, (c) beam integration, (d) convective–stratiform segregation, and (e) using different *Z-R* relationships for converting the reflectivity to rainfall intensity. The blue and orange dots show the results of complete-correction and partial-correction procedures, respectively.

Atmos. Meas. Tech. Discuss., doi:10.5194/amt-2016-388, 2016
Manuscript under review for journal Atmos. Meas. Tech.
Published: 12 December 2016

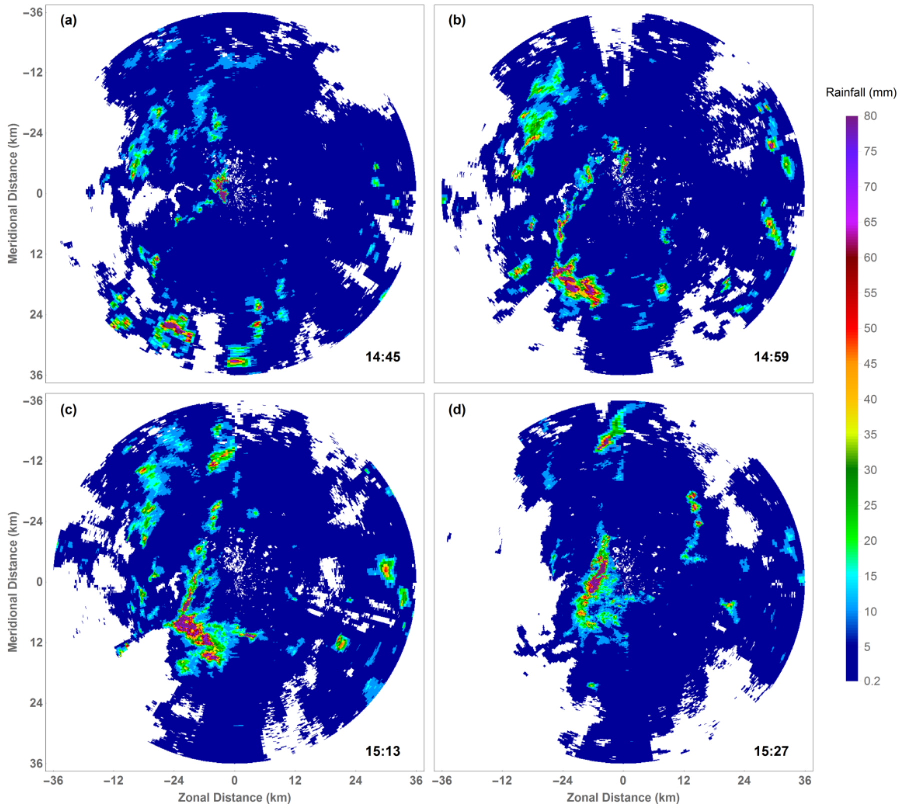

Figure 9 Snapshots of the radar-based rainfall fields for the fast-moving rainfall event of 4th September, 2015 at (a) 14:45, (b) 14:59, (c) 15:13 and (d) 15:27.

Atmos. Meas. Tech. Discuss., doi:10.5194/amt-2016-388, 2016
Manuscript under review for journal Atmos. Meas. Tech.
Published: 12 December 2016

Atmospheric Measurement Techniques Discussions
Open Access

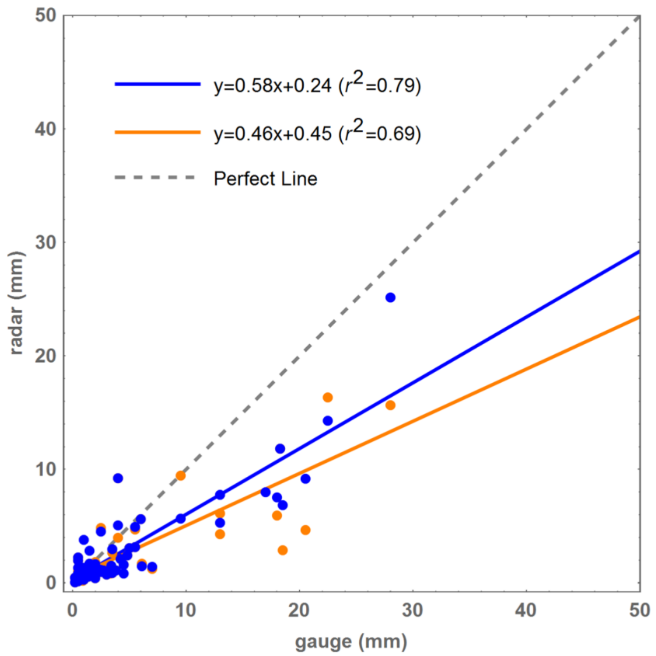

Figure 10 Performance in radar-based rainfall estimation of the wind drift correction. The blue and orange dots show the results of complete-correction and partial-correction procedures, respectively.

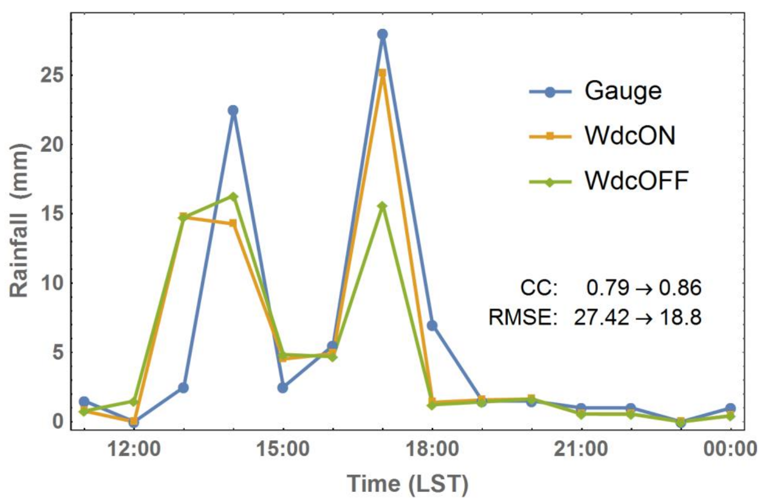

Figure 11 Rain gauge, QPE with wind drifting correction and QPE without wind

Atmos. Meas. Tech. Discuss., doi:10.5194/amt-2016-388, 2016
Manuscript under review for journal Atmos. Meas. Tech.
Published: 12 December 2016

Atmospheric Measurement Techniques Discussions
Open Access

drifting correction rainfall time series for fast-moving event, 4th-5th September 2015 at the position of closest gauge to radar.